Atmos. Chem. Phys. Discuss., 13, 26269–26303, 2013
www.atmos-chem-phys-discuss.net/13/26269/2013/
doi:10.5194/acpd-13-26269-2013

Atmospheric Chemistry and Physics Discussions

Simultaneous aerosol measurements of unusual aerosol enhancement in troposphere over Syowa Station, Antarctica

K. Hara[1], M. Hayashi[1], M. Yabuki[2], M. Shiobara[3], and C. Nishita-Hara[1]

[1]Department of Earth System Science, Faculty of Science, Fukuoka University, Fukuoka, Japan
[2]Research Institute for Sustainable Humanosphere, Kyoto University, Kyoto, Japan
[3]National Institute of Polar Research, Tokyo, Japan

Received: 12 September 2013 – Accepted: 27 September 2013 – Published: 10 October 2013

Correspondence to: K. Hara (harakei@fukuoka-u.ac.jp)

Published by Copernicus Publications on behalf of the European Geosciences Union.

Abstract

Unusual aerosol enhancement is often observed at Syowa Station, Antarctica during winter through spring. Simultaneous aerosol measurements near the surface and in the upper atmosphere were conducted twice using a ground-based optical particle counter, a balloon-borne optical particle counter, and micro-pulse LIDAR (MPL) in August and September 2012. During 13–15 August, aerosol enhancement occurred immediately after a storm condition. A high backscatter ratio and aerosol concentrations were observed from the surface to ca. 2.5 km over Syowa Station. Clouds appeared occasionally at the top of aerosol-enhanced layer during the episode. Aerosol enhancement was terminated on 15 August by strong winds caused by a cyclone's approach. In the second case on 5–7 September, aerosol number concentrations in $D_p > 0.3\,\mu m$ near the surface reached $> 10^4\,L^{-1}$ at about 15:00 UT on 5 September in spite of calm wind conditions, whereas MPL measurement exhibited aerosols were enhanced at about 04:00 UT at 1000–1500 m above Syowa Station. The aerosol enhancement occurred near the surface–ca. 4 km. In both cases, air masses with high aerosol enhancement below 2.5–3 km were transported mostly from the boundary layer over the sea-ice area. In addition, air masses at 3–4 km in the second case came from the boundary layer over the open-sea area. This air mass history strongly suggests that dispersion of sea-salt particles from the sea-ice surface contributes considerably to the aerosol enhancement in the lower free troposphere (about 3 km) and that the release of sea-salt particles from the ocean surface engenders high aerosol concentrations in the free troposphere (3–4 km).

1 Introduction

The Antarctic region, which is isolated from human activity on other continents of low latitudes and mid-latitudes, is regarded as the cleanest on the Earth. In general, aerosol number concentrations in the Antarctic coasts are lower than those in other

ACPD
13, 26269–26303, 2013

regions (e.g., Ito, 1989, 1993; Weller et al., 2011). Actually, the mean concentration of combustion-origin species such as black carbon (BC) is mainly lower than 10 ng m^{-3} at the Antarctic coasts and in inland areas (Bodhaine, 1995; Wolff et al., 1998; Pereira et al., 2006; Weller et al., 2013). The BC levels suggest that the Antarctic region remains in the cleanest of condition, although previous investigations have pointed out that BC is supplied mostly by long-range transport from biomass burning in South America, Africa, and Australia (Van den Werf et al., 2006, 2008; Fiebig et al., 2009; Hara et al., 2010). Nevertheless, haze phenomena have occurred at Syowa Station, Antarctica because of remarkable high aerosol concentrations during winter through spring in 2004–2006 (Hara et al., 2010).

Basic physical and chemical properties of the Antarctic haze (aerosol enhancement) were obtained from ground-base aerosol measurements at Syowa Station in 2004–2006 (Hara et al., 2010, 2011a) as follows. (1) Visibility dropped to < 10 km in spite of calm wind conditions and a lack of drifting snow. (2) Haze conditions are often identified immediately after storm conditions by a cyclone's approach. (3) Aerosol number concentrations near the surface increased in all size ranges (10 nm–super-µm). (4) Concentrations of combustion-origin aerosol species such as BC, NO_3^-, and organic acids increased. (5) Sea-salts were dominant aerosol species in the Antarctic haze. (6) Sea-salt particles emitted from sea-ice surface were mixed in all size ranges (D_p < 0.2, 0.2–2, and > 2 µm). Because of restrictions in logistics under severe conditions, in-situ aerosol measurements in the upper boundary layer–free troposphere in Antarctic regions have limited our knowledge of the vertical distributions of aerosols under the Antarctic haze (aerosol enhancement) conditions. Airplanes, tethered balloon, and launched balloons have been applied in several investigations of aerosol measurements in the upper boundary layer–free troposphere over Syowa Station (Hara et al., 2011b; references therein). Airplane-borne aerosol measurements conducted by Yamanouchi et al. (1999) revealed high aerosol concentrations from the surface to approximately 2300 m above sea level (a.s.l.) over Syowa Station on 30 August 1997 immediately after the storm conditions. Launched balloon-borne aerosol measurements

ACPD
13, 26269–26303, 2013

taken using an optical particle counter (OPC) on 18 June 2004 also exhibited aerosol enhancement in the surface–approximately 3000 m a.s.l. over Syowa Station (Hara et al., 2010; reference therein). Tethered balloon-borne aerosol measurements over Syowa Station in 2005 revealed that aerosols were enhanced in the boundary layer and lower free troposphere, and that sea-salt particles were dominant under the aerosol enhanced conditions (Hara et al., 2011b, 2013). These measurements provided important knowledge, especially related to the thickness of the aerosol-enhanced layer and aerosol constituents, but the time series of vertical distributions of aerosol properties under the Antarctic haze (aerosol enhancement) conditions have never been ascertained or discussed.

High aerosol number concentrations and high concentrations of sea-salt particles during Antarctic haze episodes can affect atmospheric radiation budgets and atmospheric cycles of reactive halogen species and sea-salts in the Antarctic region. To elucidate "Antarctic haze" (aerosol enhancement) and its related processes in Antarctic coasts during winter through spring, the vertical structure of the aerosol-enhanced layer must be ascertained from simultaneous aerosol measurements taken near the surface and in the upper atmosphere. This study combines ground-based aerosol measurements, remote sensing technique, and in-situ aerosol measurements in the upper boundary layer–free troposphere. This investigation was undertaken to shed light on vertical structures and features of "Antarctic haze" (aerosol enhancement) based on simultaneous aerosol measurements over Syowa Station, Antarctica.

2 Aerosol measurements and data analysis

2.1 Continuous aerosol measurements near the surface

Syowa Station (69.00° S, 39.59° E) is located on East Ongul Island in Lützow Holm Bay, ca. 4 km distant from the Prince Olav coast of Antarctica. Seasonal features of sea-ice extent off Syowa Station show a minimum around February and a maximum in

ACPD
13, 26269–26303, 2013

September–October (e.g. Comiso, 2010). The sea-ice margin on 40° E line is located at approximately 58–60° S in September–October. It is approximately 100 km distant from Syowa Station during the summer and 1000 km distant during winter through spring.

Ground-based aerosol measurements were conducted at a "Clean Air Observatory" built on the windward side, considering prevailing winds, from the main area of the station. Ambient air was taken at an air inlet ca. 5 m above the snow surface. Details of the "Clean Air Observatory" were described by Osada et al. (2006) and by Hara et al. (2010). Number concentrations and size distributions of aerosol particles were monitored using OPC (TD100; Sigma Tech.), the measurable size ranges of which were D_p (diameter) > 0.3, > 0.5, > 1.0, > 2.0, > 3.0, and > 5.0 µm. The OPC was calibrated using polystyrene latex spheres with a refractive index of 1.59–0i. Aerosol number concentrations were measured every minute (counting time for 58 s) at a flow rate of 1 L min^{-1}. Although the observatory was located on the windward side, local contamination occurs depending on wind conditions. Aerosol data were filtered to remove locally contaminated data using wind speed, wind direction, and the number concentration of condensation nuclei (CN) in accordance with criteria described by Hara et al. (2010, 2011a). Meteorological data were measured by the Japanese Meteorological Agency at the Meteorological Observatory located in the main area of the station.

2.2 MPL system and analysis

The vertical distributions of aerosols and clouds were measured continuously using micro-pulse lidar (MPL; Science & Engineering Service Inc.) at the Atmospheric Observatory in the main area of the station. The MPL is a single-channel elastic backscatter lidar with 523 nm wavelength. A diode-pumped Nd:YLF laser is vertically transmitted into the atmosphere with a repetition rate of 2500 Hz. The backscattered light from atmospheric gases and aerosol particles was received with a Schmidt–Cassegrain telescope (20 cm diameter). The field of view of the receiver is 100×10^{-6} radians. The MPL can receive a return signal from a 60 km range with a range resolution of 30 m.

ACPD
13, 26269–26303, 2013

Data were acquired in the one-minute pulse-integration mode. Details of the MPL system installed at Syowa Station were reported by Shiobara et al. (2003) and Shibata et al. (2003).

Campbell et al. (2002) outlined correction procedures for the MPL raw signal by accounting for ambient background light and instrument-specific terms. Lidar signals in the near range are affected by signal losses caused by the incomplete overlap of the laser beam and the receiver field of view. Overlap is typically resolved in experimental cases using the horizontal lidar measurement with a spatially homogeneous aerosol distribution in the target layer (Campbell et al., 2002). However, the observatory location was unsuitable for observing the horizontal sightline with no obscuration. We estimated the overlap from vertical profiles when the aerosol loading was low (i.e., the target layer is assumed to contain no aerosols). We chose a time when the backscatter through the layer was roughly assumed to be a Rayleigh signal with range by referring to the molecular backscatter intensity derived from the mean temperature and pressure profiles observed by the GPS sonde during the same season. In Antarctic regions, the aerosol optical depth (AOD) under background conditions is extremely low (Tomasi et al., 2012). The values of AOD at a wavelength of 500 nm under Antarctic background conditions are at least several times smaller than those of the Rayleigh optical depth. Therefore, this assumption does not markedly affect the derived aerosol profiles. The overlap function was estimated by fitting between the averaged lidar-returned signal under clear air conditions and the theoretical Rayleigh profile.

The aerosol backscatter ratio ($R = \beta_a + \beta_m)/\beta_m$ from the lidar signal was estimated using the backward inversion method (Fernald, 1984), where β_a and β_m respectively denote the backscatter coefficients of aerosol and molecules. This method assumes a linear relation between the aerosol extinction coefficient α_a and β_a in the form of the lidar ratio $S_1 = \alpha_a/\beta_a$. However, the lidar ratio depends on the size distribution and the refractive index of the aerosol particles as well as on the lidar wavelength. For example, the values of S_1 vary between 20 sr to 70 sr for six aerosol types (dust, polluted dust, clean marine, clean continental, pollution, and biomass burning), as defined in the

ACPD
13, 26269–26303, 2013

aerosol classification algorithms and the lidar ratio selection schemes for the Cloud–Aerosol Lidar and Infrared Pathfinder Satellite Observations (CALIPSO) aerosol products (Omar et al., 2009). However, the values of S_1 under the "Antarctic haze" condition, which are emphasized in this study, cannot be defined clearly because we have insufficient information about the aerosol optical properties in this phenomenon. Therefore, we use a fixed value of $S_1 = 30$ sr, which is close to the mean of the values for clean continental (35 sr) and clean marine (20 sr) at a wavelength of 532 nm, as reported by Omar et al. (2009). Vertical profiles of aerosol backscatter ratio were calculated for the 3 min averages of lidar data.

2.3 Measurements with balloon-borne optical particle counter

Vertical features of aerosol number concentrations and size distributions were measured using balloon-borne OPC (Yamanashi Gijutu Kobou Co. Ltd.). The balloon-borne OPC was calibrated using polystyrene latex spheres with a refractive index of 1.59–0i. For balloon-borne measurements, the measurable size range of the balloon-borne OPC was set to $D_p > 0.3$, > 0.5, > 0.8, > 1.2, > 2.0, > 3.4, > 5.0, and > 7.0 µm, which correspond to spherical particle diameters with a refractive index of 1.40–0i, and which were estimated by Mie scattering theory. Threshold sizes with refractive index 1.59–0i corresponded to $D_p > 0.26$, > 0.41, > 0.65, > 1.4, > 2.3, > 2.9, > 4.8, and > 6.5 µm. Details of the balloon-borne OPC were reported by Iwasaki et al. (2007) and Shibata et al. (2012). The balloon-borne OPC was launched simultaneously with GPS sonde (RS03G; Meisei Electric Co. Ltd.), which transmits aerosol number concentration data to the ground in addition to meteorological data and GPS data. Balloon-borne OPCs were launched from Syowa Station under aerosol-enhanced conditions near the surface at 6:55 UT on 14 August 2012 and at 14:33 UT on 6 September 2012.

ACPD
13, 26269–26303, 2013

3 Results and discussion

3.1 Aerosol enhancement on 13–15 August 2012

3.1.1 Aerosol features near the surface

Figure 1 depicts variations of aerosol number concentrations near the surface at Syowa Station during 13–16 August 2012. Because of strong winds under storm conditions, high aerosol number concentrations were observed on 13 August 2012 (DOY = 225.0–225.8). Aerosol number concentrations in $D_p > 0.3\,\mu m$ changed from ca. $4.3 \times 10^4\,L^{-1}$ to $1.1 \times 10^4\,L^{-1}$ at around 19:15 on 13 August (DOY = 225.8) when the wind speed decreased suddenly by less than $5\,m\,s^{-1}$. In spite of weak wind conditions ($< 5\,m\,s^{-1}$), the aerosol number concentrations in $D_p > 0.3\,\mu m$ increased markedly to greater than $5 \times 10^4\,L^{-1}$ at approximately 22:41 on 13 August (DOY = 225.945). Although drifting snow and fog can enhance the aerosol number concentrations, drifting snow and fog were not observed under conditions with calm winds and relative humidity lower than 83 %. Consequently, the high number concentrations might be identified as the occurrence of aerosol enhancement (Antarctic haze). As reported also by Hara et al. (2010), aerosol enhanced (Antarctic haze) conditions appeared immediately after storm conditions. Strong winds by the next cyclone approach engendered drifting snow and increased aerosol concentrations at 6:58 on 16 August (DOY = 228.3) before a drop of the aerosol number concentrations at the end of aerosol enhancement. The duration of the aerosol enhancement was estimated as 56.3 h in this case. Using the duration time and mean surface wind speeds, the horizontal scales of the Antarctic haze events were estimated as approximately 405 km.

As depicted in Fig. 1, the number concentrations increased remarkably in all size ranges during aerosol enhancement. After 10:08 on 14 August (DOY = 226.422), the number concentrations decreased gradually. Particularly, the number concentrations in larger sizes decreased significantly (e.g., approximately two order decrease in

ACPD
13, 26269–26303, 2013

$D_p > 3.0\,\mu m$). For comparison of the aerosol size distribution during aerosol enhancement, the Junge-slope was estimated in this study. The size distribution of fine–coarse particles can be approximated using the following equation (Junge, 1963).

$$\frac{dN}{d\log D_p} = \alpha D^{-\beta} \quad (1)$$

Therein, α and β respectively stand for a constant and the Junge-slope. Here, the Junge-slope (β) was estimated in the size range of 0.3–3.0 µm in diameter. The Junge slope was 3.23, on average, in the early stage of aerosol enhancement with higher number concentrations (DOY = 225.9–226.5). After DOY = 226.5, β increased gradually by ca. 4. This change might result from a significant decrease of the number concentrations in coarse mode. In general, variations of aerosol number concentrations and size distribution are controlled by formation, emission, coagulation, dry deposition, wet deposition, and size change by hygroscopicity. Because we specifically examine the aerosol number concentrations and size distribution in fine–coarse mode, contribution of new particle formation and coagulation can be negligible. Because of calm winds (mean $1.7\,m\,s^{-1}$), local aerosol emissions from snow and sea-ice surfaces were probably not significant during 14–16 August. In addition, the relative humidity changed gradually from 80 % to 70 %. Considering that the aerosol number concentrations decreased even under the extremely small change of relative humidity, the change of relative humidity cannot wholly account for the gradual decrease of the aerosol number concentrations. Consequently, it is expected that a remarkable decrease in coarse particles is associated with larger dry deposition velocity in coarse mode. To verify the contribution of dry deposition to the features of aerosol number density from 9:45 on 14 August (DOY = 226.407) until 6:25 on 16 August (DOY = 228.268), we attempt to estimate features of the aerosol number concentrations roughly by dry deposition. The relation between aerosol number concentrations and deposition velocity can be given as

$$dN = -\frac{V_{dep}}{H} N dt, \quad (2)$$

ACPD
13, 26269–26303, 2013

where N, V_{dep}, and H respectively denote the aerosol number concentration, deposition velocity, and height of the mixing layer. Then, Eq. (1) can be modified to

$$N = N_0 e^{-\frac{V_{dep}}{H}t}, \quad (3)$$

where N_0 denotes the initial number concentration. Therefore, variations of the aerosol number concentrations of each size range were fitted by an exponential decay function in this study. The fitting parameters for each size range are presented in Table 1. Vertical profiles of temperature, relative humidity, and aerosol number concentrations indicated that the height of boundary layer approximately 530 m on 14 August 2012 (details were described Sect. 3.1.2). Assuming that the height of the boundary layer was constant, V_{dep} was estimated as 1.26 cm s^{-1} in $D_p > 3$ µm, 0.55 cm s^{-1} in $D_p > 2$ µm, 0.48 cm s^{-1} in $D_p > 1$ µm, 0.38 cm s^{-1} in $D_p > 0.5$ µm, and 0.29 cm s^{-1} in $D_p > 0.3$ µm. The estimated values were well consistent with the dry deposition velocity (Grönlund et al., 2002; Seinfeld and Pandis, 2006). Therefore, the gradual decrease of aerosol number concentrations might result mostly from the dry deposition of aerosol particles during transport.

3.1.2 Aerosol features in boundarylayer–freetroposphere

Because of storm condition and snow deposition on the window of the Atmospheric Observatory for MPL measurement, vertical distributions of aerosol backscatter ratio were not obtained during the early stage of the aerosol enhancement (before 09:00 UT on 14 August), as shown in Fig. 1. Additionally, the cloud appearance and precipitation prevented identification of vertical structure of the aerosol enhancement from 14:00 UT on 14 August until 09:00 UT on 15 August (DOY = 226.6–227.3). The MPL measurements during cloud free periods over MPL on 14 and 15 August exhibited that an aerosol backscatter ratio close to 2 was observed at lower than ca. 2500 m on 14–15 August 2012. During 11:00–13:00 on 14 August (cloud-free period, DOY = 226.4–226.6), the aerosol backscatter ratio ranged in 2–3 in the boundary layer and lower free

ACPD
13, 26269–26303, 2013

troposphere (< 1500 m); it was 1.5–2 in the lower free troposphere (1500–2500 m). Although aerosols were enhanced in < 2500 m on 14 August, a thin aerosol layer with lower backscatter ratio was identified clearly at ca. 500 m and 2000 m. After the cloud disappearance at around 09:00 UT on 15 August, the aerosol-enhanced layer remained in the lower troposphere over Syowa Station. The aerosol backscatter ratio was 1.5–2.3 at altitudes lower than 2 km on 15 August. Furthermore, the height of the top of aerosol-enhanced layer descended gradually to < 1.5 km at 21:25 UT on 15 August (DOY = 227.9). Aerosol enhancement occurred from the surface to the lower free troposphere (ca. 2500 m) in this case. This thickness was similar to the thickness observed in earlier investigations by Yamanouchi et al. (1999) and Hara et al. (2011b).

Figure 2 depicts the vertical distributions of air temperature, relative humidity, aerosol number concentrations, Junge slope, and the backscatter ratio over Syowa Station on 14 August. Unfortunately, MPL data were not obtained during balloon-borne OPC measurements in this case because of snow deposition on the MPL window. Vertical features of the aerosol number concentrations in the surface–2.5 km imply the presence of several aerosol layers as follows: surface–600 m (probably a boundary layer), 700–1000 m, 1100–1600 m, and 1700–2400 m. For instance, the aerosol number concentrations of $D_p > 0.26$ µm in each layer were approximately 6.6×10^4, 1.4×10^4, 3.0×10^4, 1.4×10^4 L^{-1}, respectively. The vertical structure of aerosol number concentrations was coincident with vertical features of air temperature and the relative humidity. A similar layered structure was observed in the aerosol backscatter ratio, although MPL data were taken after several hours from the balloon-borne OPC measurements. In contrast to vertical features of aerosol number concentrations in fine mode, the number concentrations in $D_p > 2.9$, 4.8, and 6.5 µm increased gradually to 353, 252, and 171 L^{-1}, respectively, in 1100–2130 m. Particularly, the aerosol number concentrations increased in all size ranges in 2100–2200 m under conditions with higher relative humidity, so that a cloud layer appeared in this altitude. Because the aerosol number concentrations only in coarse mode was enhanced in 1600–2100 m, aerosol particles might be acti-

ACPD
13, 26269–26303, 2013

vated to cloud particles at this altitude under high relative humidity conditions. Aerosol enhanced conditions above the cloud layer were observed up to 2500 m.

The Junge-slope (β) was estimated to have sizes of 0.36–2.3 µm in diameter. The vertical feature of β also had a layered structure. In surfaces to 600 m, β was approximately 1.3. The Junge slope increased gradually from 1.3 to ca. 2 in 1000–2000 m. In the top of aerosol-enhanced layer above the cloud layer, β was 2.7–3. Because of the lower number concentration in coarse mode above the aerosol-enhanced layer, β was 2–2.5 above the aerosol-enhanced layer (above 2.5 km). According to tethered balloon-borne aerosol measurements at Syowa Station (Hara et al., 2011b), β in lower troposphere during the winter–spring, β was 1.5–2.8 (median $\beta = 2.4$). Particularly, the mean Junge slopes in the aerosol-enhanced layer in the tethered balloon-borne aerosol measurements (28 May, 22 July, and 30 September 2005) were, respectively, 2.65, 1.71, and 2.18 (Hara et al., 2011b). These ranges were similar to β in this study. However, β in ground-based OPC measurements (Fig. 1) gended to be higher than β in balloon-borne and tethered balloon borne aerosol measurements. This difference might be attributed to (1) OPC measurements under dry conditions and room temperature (ca. 20 °C) in ground-based measurements and (2) significant loss of coarse aerosol particles larger than 2 µm in diameter in the aerosol inlet of the "Clean Air Observatory".

Although measurements obtained from balloon-borne OPC and MPL were not conducted simultaneously, a higher aerosol backscatter ratio was identified from the boundary layer to the lower free troposphere (ca. 2500 m) at 10:00–13:00 UT on 14 August. A lower aerosol backscatter ratio was identified at 600 m and 1000 m during 10:00–13:00 UT. These altitudes corresponded roughly to lower aerosol number concentrations in the balloon-borne OPC measurements. Consequently, the layered structure might persist for at least several hours.

ACPD
13, 26269–26303, 2013

3.1.3 Meteorological conditions in the aerosol enhancement

Figure 3 depicts surface weather charts of Indian Ocean sector on 13–16 August 2012 (Bureau of Meteorology, Australia: http://www.bom.gov.au/index.shtml). Two cyclones approached Syowa Station on 13 August, when a storm occurred. Although the closest cyclone was located around 30° E, 68° S on 13 August, the cyclone weakened suddenly on 14 August. The sudden decline of the cyclone was observed also in cases of Antarctic haze in 2004–2006 at Syowa Station (Hara et al., 2010). Although the larger cyclone passed eastwardly around 60° S off Syowa Station on 13 August and then moved to > 50° E on 14 August, the cyclone apparently did not strongly impacted weather conditions around Syowa Station. On 15 August, Syowa Station was located in the ridge of an anticyclone. Then, the next cyclone approached Syowa Station from the west after the afternoon of 15 August. As shown in Fig. 1, the next cyclone approach caused a storm condition on 15 August at Syowa Station.

3.1.4 Air mass history of the aerosol-enhanced layer

To elucidate the air mass history of the aerosol-enhanced layer, the 5 day backward trajectory was computed from every 200 m in 200–4000 m over Syowa Station using vertical motion mode in the NOAA-HYSPLIT model with "NCEP reanalysis" data (Draxler and Rolph, 2013). Figure 4 shows examples of the 5 day backward trajectory at 03:00 UT on 14 August 2012. Air masses in the aerosol-enhanced layer travelled over sea-ice area for the prior 5 days. Air masses passed mostly lower than 1500 m over sea-ice regions. Particularly, backward trajectory from 1000–1500 m over Syowa Station showed that air masses were transported from the boundary layer (< 500 m) over a sea-ice area. Although the top of the aerosol-enhanced layer was identified clearly in MPL measurements and balloon-borne OPC measurements (Figs. 1 and 2), no significant difference was found in the transport pathway between in aerosol-enhanced layer and above the layer. Air masses in the aerosol-enhanced layer originated mostly from the boundary layer–lower free troposphere (< 1500 m) over the sea-ice area. By

ACPD
13, 26269–26303, 2013

contrast, air masses above the aerosol-enhanced layer were distributed higher than 2000 m over the sea-ice area. Considering that sea-salt particles were dominant under Antarctic haze conditions and storm conditions in our previous studies (Hara et al., 2010, 2011a), the difference strongly suggests that the aerosol-enhanced layer in the lower troposphere was associated with a release of aerosol particles from the sea-ice surface. Strong winds attributable to a cyclone approach might cause a considerable dispersion of sea-salt particles from the sea-ice surface. Then, a sudden decline of a cyclone like that shown in Fig. 3 can maintain conditions with marked dispersion of sea-salt particles (i.e. aerosol enhancement) in the surface – lower free troposphere.

As described above, the top of aerosol-enhanced layer descended gradually on 15 August, when Syowa Station was located in a high-pressure ridge (shown in Fig. 3). The backward trajectory indicated that air masses above the aerosol-enhanced layer on 15 August derived from the free troposphere (> 3500 m) over the Weddell Sea and Antarctic Peninsula (Fig. 4b). In contrast, air masses in the aerosol-enhanced layer on 15 August travelled in the lower troposphere (< 2000 m) over sea-ice and Antarctic coast around Syowa Station. Therefore, a gradual descent of the top of the layer might result from (1) location of a high-pressure ridge and (2) transport of clean air in the free troposphere over Syowa Station.

3.2 Aerosol enhancement on 6 September 2012

3.2.1 Aerosol features near the surface

Figure 5 depicts variations of aerosol number concentrations near the surface at Syowa Station during 4–7 September 2012 (DOY = 247.0–251.0). Although aerosol enhancements in the cases of August 2012 (Sect. 3.1) and previous investigation (Hara et al., 2010) occurred immediately after the storm conditions, the wind speed near the surface was $< 5\,m\,s^{-1}$ before the aerosol enhancement in this case. This difference is interesting to elucidate the origin and transport processes of Antarctic haze and the aerosol-enhanced layer. In addition, the aerosol number concentrations dropped before aerosol

ACPD
13, 26269–26303, 2013

enhancement because of slight precipitation near the surface during the DOY = 248.0–248.5. Then, the aerosol number concentrations in $D_p > 0.3\,\mu m$ increased gradually and exceeded $10^4\,L^{-1}$ at 15:04 on August (DOY = 248.7), when the relative humidity and air temperature respectively started to decrease and increase simultaneously. Those simultaneous changes suggest that a "front-like" structure passed over Syowa Station. Aerosol number concentrations in $D_p > 0.3\,\mu m$ reached $3.7 \times 10^4\,L^{-1}$ during aerosol enhancement, although the number concentrations in $D_p > 2.0$ and $3.0\,\mu m$ were, respectively, 20–170 L^{-1} (mean, 106 L^{-1}) and $< 2\,L^{-1}$ (mean, 0.4 L^{-1}). Although the number concentrations of $D_p > 0.3\,\mu m$ resembled those on 14–16 August, the number concentrations in $D_p > 2.0$ and $3.0\,\mu m$ were several factor or one orders smaller than those on 14–16 August (Fig. 1). As a result, the Junge slope was of a higher range (3.7–4.8; mean, 4.3) than the Junge slope (3.0–4.5; mean, 3.6) on 14–16 August. Aerosol enhancement ($10^4\,L^{-1}$ in $D_p > 0.3\,\mu m$) remained near the surface until 08:00 UT 7 September (DOY = 250.3). Unlike the sudden decrease of aerosol number concentrations in the cases described in Hara et al. (2010), the number concentrations in $D_p > 0.3\,\mu m$ decreased gradually to $< 10^4\,L^{-1}$. The duration of the aerosol enhancement was identified as 40.9 h. The horizontal scale of the aerosol enhancement was estimated approximately to 255 km using mean surface wind speeds.

3.2.2 Aerosol features in the boundary layer–free troposphere

As shown in Fig. 5, the aerosol-enhanced layer were not observed before 13:00 UT on 4 September (DOY = 247.5). After 14:00 UT on 4 September, the aerosol backscatter ratio increased slightly by 1.4 in the boundary layer and in the lower free troposphere (< 4 km). Remarkable aerosol enhancement started below 1 km at 01:00 UT on 5 September (DOY = 248.04). The top altitude of aerosol-enhanced layer rose gradually to ca. 2.7 km on 5 September. Particularly, the aerosol backscatter ratio exceeded 4 at 1–1.8 km during 12:00–13:30 UT on 5 September. Remarkable aerosol enhancement remained on 6 September. The top of the aerosol-enhanced layer was

ACPD
13, 26269–26303, 2013

identified in ca. 2.7 km on 6 September. Moreover, the aerosol-enhanced layer with aerosol backscatter ratio larger than 2 was expanded up to ca. 4 km until 08:00 UT on 6 September (DOY = 249.33). After 03:00 UT on 6 September (DOY = 249.13), the aerosol backscatter ratio decreased to less than 2 below 1 km. Considering that the top of the boundary layer was usually < 1000 m in August (Hara et al., 2011b), Antarctic haze (aerosol enhanced condition) might be distributed not only near the surface and boundary layer, but also in the lower free troposphere over Syowa Station. Aerosol enhancement at altitudes higher than 2 km was terminated approximately at 13:00 UT on 6 September (DOY = 249.54), although the aerosol-enhanced layer thickness became markedly less at altitudes lower than 2 km. The aerosol backscatter ratio decreased gradually in the lower free troposphere. Then, aerosol enhancement above 1 km remained until 22:00 UT on 6 September (DOY = 249.92).

Figure 6 depicts vertical distributions of air temperature, relative humidity, aerosol number concentrations, Junge slope, and aerosol backscatter ratio over Syowa Station on 6 September. Similarly to the case on 14 August, several layered structures were identified. Vertical features of the aerosol number concentrations in surface–4 km imply the presence of several aerosol layers as follows: surface–1000 m (probably a boundary layer), 1000–1500 m, 1600–2200 m, 2300–2600, 2700–3100 m, 3200–3800, and > 3800 m. The respective aerosol number concentrations in $D_p > 0.26$ µm in the layers were approximately 3.0×10^4–4.3×10^4 L^{-1}, 8.8×10^4 L^{-1}, 5.0×10^4 L^{-1}, 2.7×10^4 L^{-1}, 5.8×10^4 L^{-1}, 2.7×10^4 L^{-1}, and 8×10^3 L^{-1}. The layered structures of aerosol number concentrations corresponded well to vertical features of air temperature and the relative humidity. Balloon-borne OPC measurements were taken on 6 September during the decline of aerosol enhancement. Considerable aerosol enhancement was found in the lower free troposphere (1000–1600 m). Actually, higher number concentrations were found, respectively, at 1000–1600 m, for instance 9.0×10^4 L^{-1} and 575 L^{-1} in $D_p > 0.26$ µm and > 2.3 µm. Furthermore, a higher aerosol backscatter ratio (2.1–2.3) was observed at that altitude. High number concentrations in balloon-borne aerosol measurements were obtained up to ca. 3100 m, although a slight decrease of aerosol

ACPD
13, 26269–26303, 2013

number concentrations was observed at 2300–2600 m. In contrast to aerosol enhancement in August, the margin of the top of aerosol-enhanced layer was not clear in this case. Above 3200 m, the aerosol number concentrations decreased gradually with altitude. Vertical features of the hourly mean backscatter ratio at 14:00–15:00 UT were well coincident with the vertical distributions of aerosol number concentrations.

Furthermore, the number concentrations of $D_p > 2.3\,\mu m$ in surface–4 km on 6 September were one–two orders lower than those on 14 August, although the number concentrations of fine mode (e.g., $D_p > 0.26\,\mu m$) in this case were similar or higher relative to the case on 14 August. As a result, the Junge slope was 1.9–2.7 below 3100 m on 6 September. Similarly to near the surface, the Junge slope in the upper boundary layer – free troposphere on 6 September was greater than that on 14 August. The lowest Junge slope (1.9–2.0) was observed in the aerosol-enhanced layer in 1000–1600 m, where the aerosol number concentrations in coarse mode were one order higher than either below or above the aerosol-enhanced layer. The Junge slope increased gradually in 3100–4000 m because of the gradual decrease of aerosol number concentrations in coarse mode. As discussed above, a higher Junge slope on 6 September might result from the dry deposition of coarse particles during transport. This difference in Junge slope implies that air masses on 6 September were aged relative to the air mass on 14 August. Details are discussed in Sect. 3.2.4.

3.2.3 Meteorological field in the aerosol enhancement

Figure 7 depicts surface weather charts of the Indian Ocean sector during 4–7 September (Bureau of Meteorology, Australia: http://www.bom.gov.au/index.shtml). Before aerosol enhancement on 4 September, Syowa Station was located in the ridge of anticyclone. The cyclone located around 55° E, 65° S at 00:00 UT on 4 September suddenly weakened also in this case. Considering isobar distributions around Syowa Station before the occurrence of the aerosol enhancement, poleward flow might occur in 70–80° E. The cyclone passed eastwardly around 55° S off Syowa Station on 5 September. Syowa Station, however, was located under high-pressure conditions

ACPD
13, 26269–26303, 2013

on 5–6 September. Although the aerosol number concentrations in $D_p > 0.3\,\mu m$ decreased to $< 10^4\,L^{-1}$ on 7 September, Syowa Station remained located in the ridge of high pressure.

3.2.4 Air mass history of the aerosol-enhanced layer

Figure 8 portrays examples of 5 day backward trajectory during aerosol enhancement on 5–7 September. Air masses of the aerosol-enhanced layer (below 2400 m a.s.l.) at 00:00 UT on 6 September (DOY = 249.00) were transported from the boundary layer via sea-ice regions and coastal line. Poleward flow from < 60° S occurred along ca. 90° E line on 2–3 September. End-points of the 5 day backward trajectory from the aerosol-enhanced layer were distributed around 45–65° S. According to Comiso (2010), the sea-ice area in September was usually extended to ca. 60° S on 70–90° E. Therefore, air masses came from the boundary layer (< 1000 m) over sea-ice and open sea areas. By contrast, air masses above 2400 m indicate transport above ca. 1000 m (probably free troposphere) over sea-ice regions. This height of transport was well consistent with vertical features of aerosol backscatter ratio. After air masses reached near the coasts on 3 September, aerosol-enhanced air moved slowly to Syowa Station, especially during 4–6 September.

As shown in Fig. 5, a high aerosol backscatter ratio was observed above 3 km for ca. 11 h on 6 September. Five-day backward trajectory from the aerosol-enhanced layer at 04:00 UT on 6 September (DOY = 249.166) showed a similar transport pathway from sea-ice and open sea areas. Especially, air masses above 3 km were transported from the boundary layer over the open sea area (< 50° S). Air masses of the aerosol-enhanced layer above 3 km were located at altitudes higher than 1300 m over 60° S (near sea-ice margin). Therefore, the travel time in the boundary layer over the sea-ice area might be shorter. By contrast, the travel time in the boundary layer over the sea-ice area was likely to be longer in the air masses of aerosol-enhanced layer below 3 km.

ACPD
13, 26269–26303, 2013

Poleward flow over sea-ice regions suggests that large amounts of sea-salt particles were released from surfaces of ocean and sea-ice under strong wind conditions on 2–3 September. Consequently, the dispersion of sea-salt particles from sea-ice and open sea surfaces might contribute considerably to aerosol enhancement below 3 km during 5–7 September, similar to the aerosol enhancement on August 2012 and the other cases (Hara et al., 2010). Considering the vertical motion over sea-ice area during transport and considering the vertical features of the aerosol backscatter ratio, the release of sea-salt particles from the sea-ice surface and open sea surface might respectively engender aerosol enhancement below 2.7 km and in 2.7–4 km. Particularly, the dispersion of sea-salt particles from sea-ice is expected to make a significant contribution to strong aerosol enhancement below 2.7 km. Sea-salt particles were released only slightly from the sea-ice surface under calm wind conditions. Therefore, the concentrations of the dispersed sea-salt particles might decrease gradually through dry deposition during westward transport along the coasts. This likelihood is consistent with the lower concentrations in $D_p > 2.0$ and 3.0 µm in this case, as described above.

After 13:00 UT on 6 September (DOY = 249.54), the aerosol-enhanced layer became thinner, as shown in Figs. 5 and 7. Backward trajectory results indicated that air masses above the aerosol-enhanced layer (> 1800 m) travelled mostly at altitudes higher than 2000 m over the sea-ice area. In addition, the air mass origin and transport pathways were shifted gradually over the Antarctic continent. On 7 September, the origin of the air mass above 2000 m moved to the free troposphere over the Antarctic continent (not shown). Therefore, transport of clean air from the free troposphere might cause termination of the aerosol enhancement in the free troposphere over Syowa Station.

3.3 Implications of aerosol enhancement in the lower troposphere

Dispersion of sea-salt particles from sea-ice surface contributed significantly to aerosol enhancement in the lower troposphere over Syowa Station. Particularly sea-ice origin sea-salt particles were distributed mostly at altitudes lower than 2.5 km in both cases. This vertical distribution provides important evidence to ascertain atmospheric cycles

ACPD
13, 26269–26303, 2013

of sea-salt particles in the Antarctic regions and to infer results from ice core record data. Sea-salt has often been used as an index of sea-ice extent in ice core records (e.g., Wolff et al., 2006). Sea-salt particles originated from sea-ice are fractionated in winter–spring, as suggested by Hara et al. (2012) and references in that report. Although the presence of the fractionated sea-salt particles was identified in inland areas (Hara et al., 2004; Udisti et al., 2012), transport processes of sea-salt particles from sea-ice areas to inland areas have not been discussed well. To elucidate the transport processes of sea-salt particles derived from sea-ice in the aerosol-enhanced layer, we calculated 5 day forward trajectory from the aerosol-enhanced layer in August and September over Syowa Station (not shown). The trajectories in both cases indicated that air parcels were transported not to inland areas but to the boundary layer over sea-ice and open-sea areas. Because only two cases were discussed in this study, we cannot conclude whether sea-salt particles from sea-ice in the aerosol-enhanced layer were usually transported to inland areas, or not. As described earlier, the aerosol-enhanced layer was observed at altitudes lower than ca. 2.7 km in this study. This altitude is useful as an index to discuss transport of sea-salt particles from sea-ice and coastal areas to inland areas if aerosol enhancement by dispersion of sea-salt particles from sea-ice occurs usually at altitudes lower than 2.7 km around the Antarctic coasts. Indeed, air masses with high sea-salt concentrations (Na^+) at Dome F were located in the lower free troposphere (1600–3500 m) over the coastal line (Hara et al., 2004).

As described above, large amounts of sea-salt particles, especially those released from sea-ice surfaces, were present in the aerosol-enhanced layer. The marked enhancement of sea-salt particles can induce substantial release of reactive halogen species through heterogeneous reactions (e.g., Simpson et al., 2007; Saiz-Lopez et al., 2008). Reactive halogen species such as BrO and Br relate closely to ozone depletion and the oxidation of dimethylsulfide in the lower troposphere (e.g., Simpson et al., 2007; Saiz-Lopez et al., 2008; Read et al., 2008). Actually, our previous work indicated that O_3 concentrations near the surface dropped simultaneously during the Antarctic haze after polar sunrise (Hara et al., 2010). In addition, O_3 depletion in coastal Antarc-

ACPD
13, 26269–26303, 2013

tic region was extended upward to ca. 3 km (Wessel et al., 1998; Jones et al., 2010). The vertical extent of O_3 depletion corresponded approximately to the vertical structure of the aerosol-enhanced layer in this study. Therefore, it is expected that aerosol enhancement (Antarctic haze) with large amounts of sea-salt particles in the lower troposphere plays important roles in atmospheric chemical cycles that prevail along the Antarctic coasts.

Aerosol enhancement conditions were produced by the substantial release of sea-salt particles from the ocean and sea-ice surfaces under strong winds during transport. Poleward flow can engender the transport of humid air into Antarctic coasts along with mixing of large amounts of sea-salt particles. During aerosol enhancement, clouds appeared occasionally in the upper boundary layer and lower free troposphere. Considering the significant transport of water vapor by poleward flow and dispersion of sea-salt particles in the aerosol-enhanced layer, cloud activation might be promoted in the aerosol-enhanced layer. Antarctic haze can occur on other Antarctic coasts. Therefore, cloud appearance in the Antarctic haze might affect atmospheric radiation budgets temporarily in coastal Antarctic regions.

4 Concluding remarks

Simultaneous aerosol measurements were taken twice on 14 August and 6 September 2012 at Syowa Station, Antarctica using ground-based OPC, balloon-borne OPC, and MPL under aerosol-enhanced conditions. Remarkable aerosol enhancement was identified in the boundary–lower free troposphere (near the surface–2.7 km) in both cases. Moreover, high aerosol number concentrations and an aerosol backscatter ratio were observed up to ca. 4 km on 6 September. In both cases, aerosol enhancement was likely to be associated with large amounts of sea-salt particles from sea-ice and ocean surfaces under strong winds during poleward flow by a cyclone approach. Particularly, dispersion of sea-salt particles from sea-ice surface might make an important contribution to the occurrence of aerosol enhancement near the surface to 2.7 km.

ACPD
13, 26269–26303, 2013

Aerosol enhancement (Antarctic haze) can affect atmospheric material cycles and atmospheric chemistry in coastal regions of Antarctica. The twice simultaneous measurements in this study, however, are too short to elucidate the occurrence of Antarctic haze, or to estimate its contribution quantitatively. For better understanding, it is necessary to obtain more knowledge about the vertical structure of aerosol-enhanced layer, their seasonal features, and transport processes in the troposphere over the Antarctic coasts.

Acknowledgements. We would like to thank C. Ikeda, T. Fujita, and other JARE53 wintering members for field operations at Syowa Station, Antarctica. The authors gratefully acknowledge the NOAA Air Resources Laboratory (ARL) for the provision of the HYSPLIT transport and dispersion model and/or READY website (http://ready.arl.noaa.gov) used in this publication. This work was also supported by a Grant-in-Aid for Scientific Research (B) (No.22310013, PI: K. Hara) from the Ministry of Education, Culture, Sports, Science and Technology of Japan.

References

Bodhaine, B. A.: Aerosol absorption measurements at Barrow, Mauna Loa and the South Pole, J. Geophys. Res., 100, 8967–8975, 1995.

Comiso, J.: Characteristics and variability of the sea ice cover, in: Polar Oceans from Space, Springer, New York, USA, 295–363, 2010.

Campbell, J. R., Hlavka, D. L., Welton, E. J., Flynn, C. J., Turner, D. D., Spinhirne, J. D., Scott, V. S., and Hwang, I. H.: Full-time, eye-safe cloud and aerosol lidar observation at atmospheric radiation measurement program sites: instruments and data processing, J. Atmos. Ocean. Technol., 19, 431–442, 2002.

Draxler, R. R. and Rolph, G. D.: HYSPLIT (HYbrid Single-Particle Lagrangian Integrated Trajectory) Model access via NOAA ARL READY Website, available at: http://ready.arl.noaa.gov/HYSPLIT.php, NOAA Air Resources Laboratory, Silver Spring, MD, 2013

Fernald, F. G.: Analysis of atmospheric lidar observations: some comments, Appl. Optics, 23, 652–653, 1984.

ACPD

13, 26269–26303, 2013

Fiebig, M., Lunder, C. R., and Stohl, A.: Tracing biomass burning aerosol from South America to Troll Research Station, Antarctica, Geophys. Res. Lett., 36, L14815, doi:10.1029/2009GL038531, 2009.

Grönlund, A., Nilsson, D., Koponen, I. K., Virkkula, A., and Hansson, M.: Aerosol dry deposition measured with eddy-covariance technique at Wasa and Aboa, Dronning Maud Land, Antarctica, Ann. Glaciol., 35, 355–361, 2002.

Hara, K., Osada, K., Yabuki, M., Hashida, G., Yamanouchi, T., Hayashi, M., Shiobara, M., Nishita-Hara, C., and Wada, M.: Haze episodes at Syowa Station, coastal Antarctica: where did they come from?, J. Geophys. Res., 115, D14205, doi:10.1029/2009JD012582, 2010.

Hara, K., Osada, K., Nishita-Hara, C., Yabuki, M., Hayashi, M., Yamanouchi, T., Wada, M., and Shiobara, M.: Seasonal features of ultrafine particle volatility in the coastal Antarctic troposphere, Atmos. Chem. Phys., 11, 9803–9812, doi:10.5194/acp-11-9803-2011, 2011a.

Hara, K., Osada, K., Nishita-Hara, C., and Yamanouchi, T.: Seasonal variations and vertical features of aerosol particles in the Antarctic troposphere, Atmos. Chem. Phys., 11, 5471–5484, doi:10.5194/acp-11-5471-2011, 2011b.

Hara, K., Osada, K., Yabuki, M., and Yamanouchi, T.: Seasonal variation of fractionated sea-salt particles on the Antarctic coast, Geophys. Res. Lett., 39, L18801, doi:10.1029/2012GL052761, 2012.

Hara, K., Osada, K., and Yamanouchi, T.: Tethered balloon-borne aerosol measurements: seasonal and vertical variations of aerosol constituents over Syowa Station, Antarctica, Atmos. Chem. Phys., 13, 9119–9139, doi:10.5194/acp-13-9119-2013, 2013.

Ito, T.: Antarctic submicron aerosols and long-range transport of pollutants, Ambio, 18, 34–41, 1989.

Ito, T.: Size distribution of Antarctic submicron aerosols, Tellus B, 45, 145–159, doi:10.1034/j.1600-0889.1993.t01-1-00007.x, 1993.

Iwasaki, S., Maruyama, K., Hayashi, M., Ogino, S.-Y., Ishimoto, H., Tachibana, Y., Shimizu, A., Matsui, I., Sugimoto, N., Yamashita, K., Saga, K., Iwamoto, K., Kamiakito, Y., Chabangborn, A., Thana, B., Hashizume, M., Koike, T., and Oki, T.: Characteristics of aerosol and cloud particle size distributions in the tropical tropopause layer measured with optical particle counter and lidar, Atmos. Chem. Phys., 7, 3507–3518, doi:10.5194/acp-7-3507-2007, 2007.

Jones, A. E., Anderson, P. S., Wolff, E. W., Roscoe, H. K., Marshall, G. J., Richter, A., Brough, N., and Colwell, S. R.: Vertical structure of Antarctic tropospheric ozone deple-

ACPD
13, 26269–26303, 2013

tion events: characteristics and broader implications, Atmos. Chem. Phys., 10, 7775–7794, doi:10.5194/acp-10-7775-2010, 2010.
Junge, C. E.: Aerosols, in: Air Chemistry and Radioactivity, Academic Press, 111–208, 1963.
Osada, K., Hayashi, M., Shiobara, M., Hara, K., Wada, M., Hashida, G., Morimoto, S., Yabuki, M., and Yamanouchi, T.: Atmospheric observation room for clean air at Syowa Station, East Antarctica, Antarctic Records, 50, 86–102, 2006 (in Japanese).
Omar, A. H., Winker, D. M., Kittaka, C., Vaughan, M. A., Liu, Z., Hu, Y., Trepte, C. R., Rogers, R. R., Ferrare, R. A., Lee, K.-P., Kuehn, R. E., and Hostetler, C. A.: The CALIPSO automated aerosol classification and lidar ratio selection algorithm, J. Atmos. Ocean. Technol., 26, 1994–2014, 2009.
Pereira, E. B., Evangelista, H., Pereira, K. C. D., Cavalcanti, I. F. A., and Setzer, A. W.: Apportionment of black carbon in the South Shetland Islands, Antarctic Peninsula, J. Geophys. Res., 111, D03303, doi:10.1029/2005JD006086, 2006.
Read, K. A., Lewis, A. C., Bauguitte, S., Rankin, A. M., Salmon, R. A., Wolff, E. W., Saiz-Lopez, A., Bloss, W. J., Heard, D. E., Lee, J. D., and Plane, J. M. C.: DMS and MSA measurements in the Antarctic Boundary Layer: impact of BrO on MSA production, Atmos. Chem. Phys., 8, 2985–2997, doi:10.5194/acp-8-2985-2008, 2008.
Saiz-Lopez, A., Plane, J. M. C., Mahajan, A. S., Anderson, P. S., Bauguitte, S. J.-B., Jones, A. E., Roscoe, H. K., Salmon, R. A., Bloss, W. J., Lee, J. D., and Heard, D. E.: On the vertical distribution of boundary layer halogens over coastal Antarctica: implications for O_3, HO_x, NO_x and the Hg lifetime, Atmos. Chem. Phys., 8, 887–900, doi:10.5194/acp-8-887-2008, 2008.
Seinfeld, J. H. and Pandis, S. N., Dry deposition, in: Atmospheric Chemistry and Physics from Air Pollution to Climate Change, 2nd edn., Wiley-Interscience Publication, New Jersey, pp. 900–931, 2006.
Shiobara, M., Yabuki, M., and Kobayashi, H.: A polar cloud analysis based on Micro-pulse Lidar measurements at Ny-Ålesund, Svalbard and Syowa, Antarctica, Phys. Chem. Earth, 28, 1205–1212, 2003.
Shibata, T., Sato, K., Kobayashi, H., Yabuki, M., and Shiobara, M., Antarctic polar stratospheric clouds under temperature perturbation by nonorographic inertia gravity waves observed by micropulse lidar at Syowa Station, J. Geophys. Res., 108, 4105, doi:10.1029/2002JD002713, 2003.

ACPD
13, 26269–26303, 2013

Shibata, T., Hayashi, M., Naganuma, A., Hara, N., Hara, K., Hasebe, F., Shimizu, K., Komala, N., Inai, Y., Vömel, H., Hamdi, S., Iwasaki, S., Fujiwara, M., Shiotani, M., Ogino, S.-Y. and Nishi, N.: Cirrus cloud appearance in a volcanic aerosol layer around the tropical cold point tropopause over Biak, Indonesia, in January 2011, J. Geophys. Res., 117, D11209, doi:10.1029/2011JD017029, 2012.

Simpson, W. R., von Glasow, R., Riedel, K., Anderson, P., Ariya, P., Bottenheim, J., Burrows, J., Carpenter, L. J., Frieß, U., Goodsite, M. E., Heard, D., Hutterli, M., Jacobi, H.-W., Kaleschke, L., Neff, B., Plane, J., Platt, U., Richter, A., Roscoe, H., Sander, R., Shepson, P., Sodeau, J., Steffen, A., Wagner, T., and Wolff, E.: Halogens and their role in polar boundary-layer ozone depletion, Atmos. Chem. Phys., 7, 4375–4418, doi:10.5194/acp-7-4375-2007, 2007.

Tomasi, C., Lupi, A., Mazzola, M., Stone, R. S., Dutton, E. G., Herber, A., Radionov, V. F., Holben, B. N., Sorokin, M. G., Sakerin, S. M., Terpugova, S. A., Sobolewski, P. S., Lanconelli, C., Petkov, B. H., Busetto, M., and Vitale, V.: An update on polar aerosol optical properties using POLAR-AOD and other measurements performed during the International Polar Year, Atmos. Environ., 52, 29–47, 2012.

Udisti, R., Dayan, U., Becagli, S., Busetto, M., Frosini, D., Legrand, M., Lucarelli, F., Preunkert, S., Severi, M., Traversi, R., and Vitale, V.: Sea spray aerosol in central Antarctica, Present atmospheric behaviour and implications for paleoclimatic reconstructions, Atmos. Environ., 52, 109–120, 2012.

van der Werf, G. R., Randerson, J. T., Giglio, L., Collatz, G. J., Kasibhatla, P. S., and Arellano Jr., A. F.: Interannual variability in global biomass burning emissions from 1997 to 2004, Atmos. Chem. Phys., 6, 3423–3441, doi:10.5194/acp-6-3423-2006, 2006.

Van der Werf, G. R., Randerson, J. T., Giglio, L., Gobron, N., and Dolman, A. J.: Climate controls on the variability of fires in the tropics and subtropics, Global Biogeochem. Cy., 22, GB3028, doi:10.1029/2007GB003122, 2008.

Weller, R., Minikin, A., Wagenbach, D., and Dreiling, V.: Characterization of the inter-annual, seasonal, and diurnal variations of condensation particle concentrations at Neumayer, Antarctica, Atmos. Chem. Phys., 11, 13243–13257, doi:10.5194/acp-11-13243-2011, 2011.

Weller, R., Minikin, A., Petzold, A., Wagenbach, D., and König-Langlo, G.: Characterization of long-term and seasonal variations of black carbon (BC) concentrations at Neumayer, Antarctica, Atmos. Chem. Phys., 13, 1579–1590, doi:10.5194/acp-13-1579-2013, 2013.

ACPD
13, 26269–26303, 2013

Wessel, S., Aoki, S., Winkler, P., Weller, R., Herber, A., Gernandt, H., and Schrems, O.: Tropospheric ozone depletion in polar regions. A comparison of observations in the Arctic and Antarctic, Tellus B, 50, 34–50, doi:10.1034/j.1600-0889.1998.00003.x, 1998.

Wolff, E. W. and Cachier, H.: Concentrations and seasonal cycle of black carbon in aerosol at a coastal Antarctic station, J. Geophys. Res., 103, 11033–11042, doi:10.1029/97JD01363, 1998.

Wolff, E. W., Fischer, H., Fundel, F., Ruth, U., Twarloh, B., Littot, G. C., Mulvaney, R., Röthlisberger, R., de Angelis, M., Boutron, C. F., Hansson, M., Jonsell, U., Hutterli, M. A., Lambert, F., Kaufmann, P., Stauffer, B., Stocker, T. F., Steffensen, J. P., Bigler, M., Siggaard-Andersen, M. L., Udisti, R., Becagli, S., Castellano, E., Severi, M., Wagenbach, D., Barbante, C., Gabrielli, P., and Gaspari, V.: Southern Ocean sea-ice extent, productivity and iron flux over the past eight glacial cycles, Nature, 440, 491–496, doi:10.1038/nature04614, 2006.

Yamanouchi, T., Wada, M., Fukatsu, T., Hayashi, M., Osada, K., Nagatani, M., Nakata, A., and Iwasaka, Y.: Airborne observation of water vapor and aerosols along Mizuho route, Antarctica, Polar Meteorol. Glaciol., 13, 22–37, 1999.

ACPD
13, 26269–26303, 2013

Table 1. Fitting parameters in the exponential decay for aerosol number concentrations of each size range from 9:45 on 14 August (DOY = 226.407) until 6:25 on 16 August (DOY = 228.268).

Size range	a^*	b^*	R^2
$D_p > 3\,\mu m$	7.160	2.537×10^{-5}	0.8543
$D_p > 2\,\mu m$	3.439×10^{2}	1.043×10^{-5}	0.8518
$D_p > 1\,\mu m$	1.397×10^{3}	9.089×10^{-6}	0.8496
$D_p > 0.5\,\mu m$	9.563×10^{3}	7.133×10^{-6}	0.8910
$D_p > 0.3\,\mu m$	3.337×10^{4}	5.468×10^{-6}	0.9141

* Exponential decay function is "$y = a\,e^{-bx}$".

ACPD
13, 26269–26303, 2013

Simultaneous aerosol measurements of unusual aerosol enhancement

K. Hara et al.

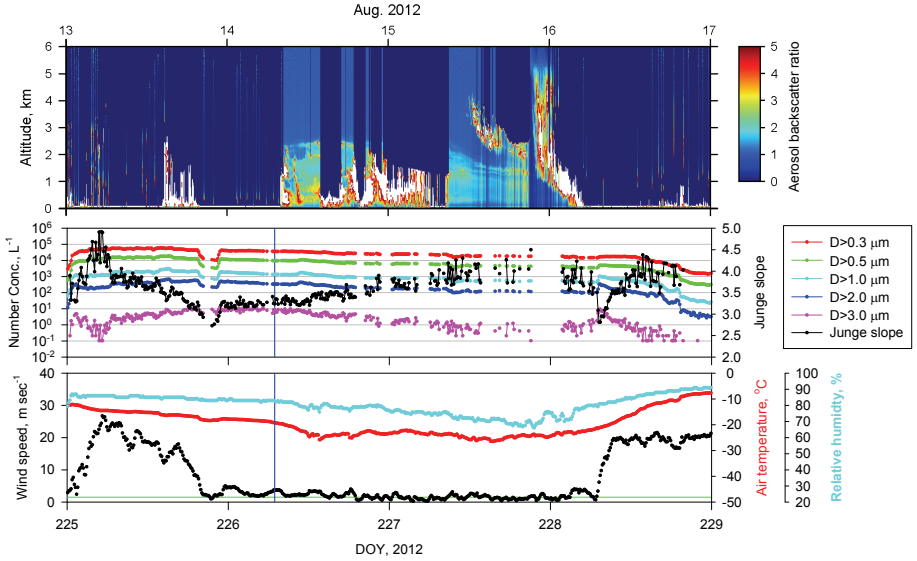

Fig. 1. Short-term variation of aerosol backscatter ratio, aerosol number concentrations near the surface, wind speed, air temperature, and relative humidity on 13–16 August 2012 at Syowa Station, Antarctica.

ACPD
13, 26269–26303, 2013

Simultaneous aerosol measurements of unusual aerosol enhancement

K. Hara et al.

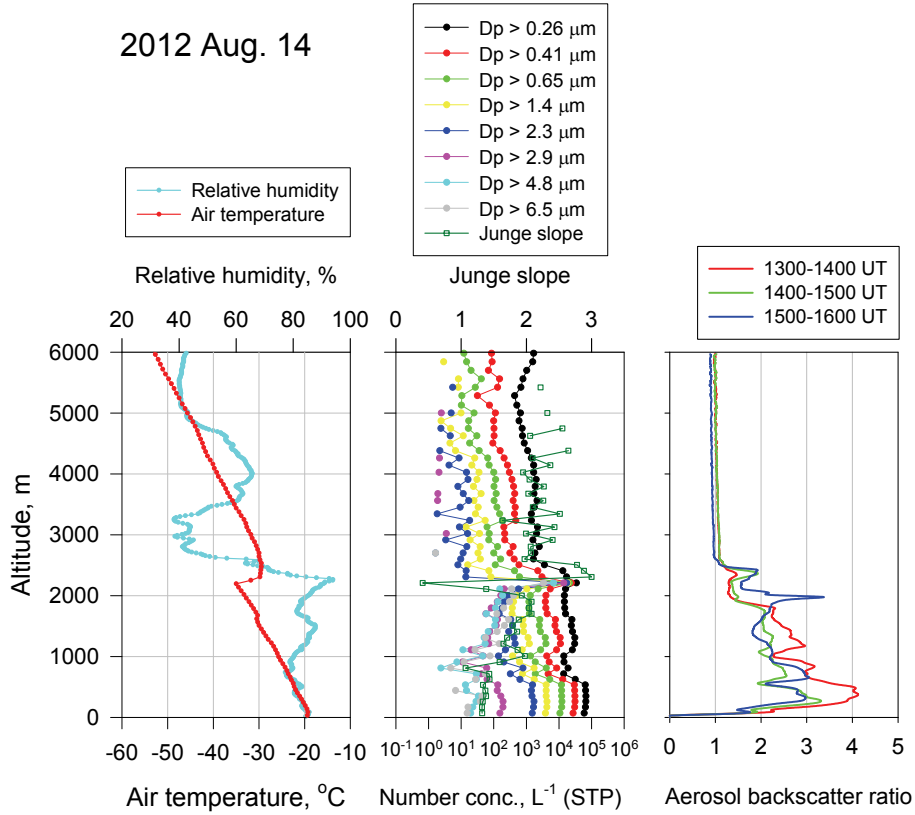

Fig. 2. Vertical variations of air temperature, relative humidity, aerosol number concentrations, Junge slope, and backscatter ratio over Syowa Station on 14 August 2012.

ACPD
13, 26269–26303, 2013

Simultaneous aerosol measurements of unusual aerosol enhancement

K. Hara et al.

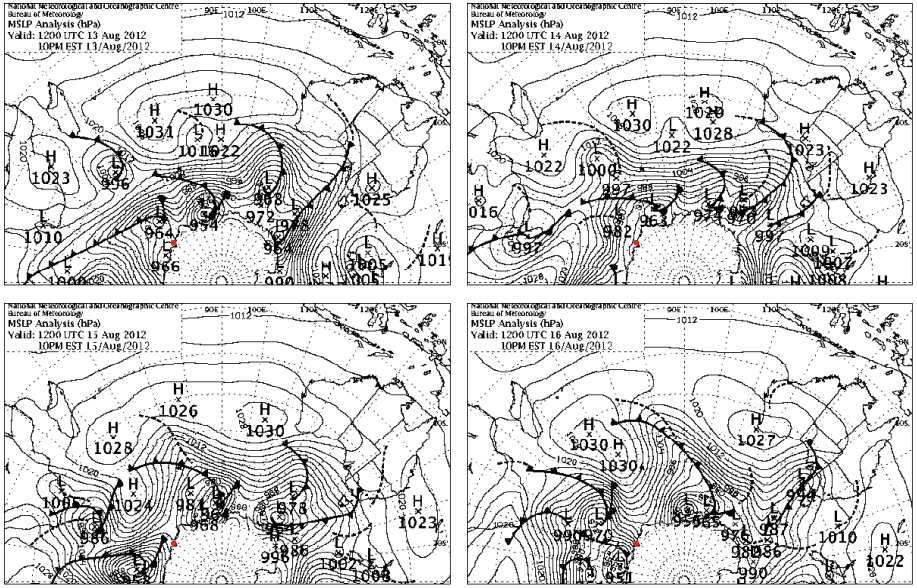

Fig. 3. Surface weather charts of the Indian Ocean sector on 13–16 August 2012 (Bureau of Meteorology, Australia: http://www.bom.gov.au/index.shtml). Red circles represent the Syowa Station location.

ACPD
13, 26269–26303, 2013

Simultaneous aerosol measurements of unusual aerosol enhancement

K. Hara et al.

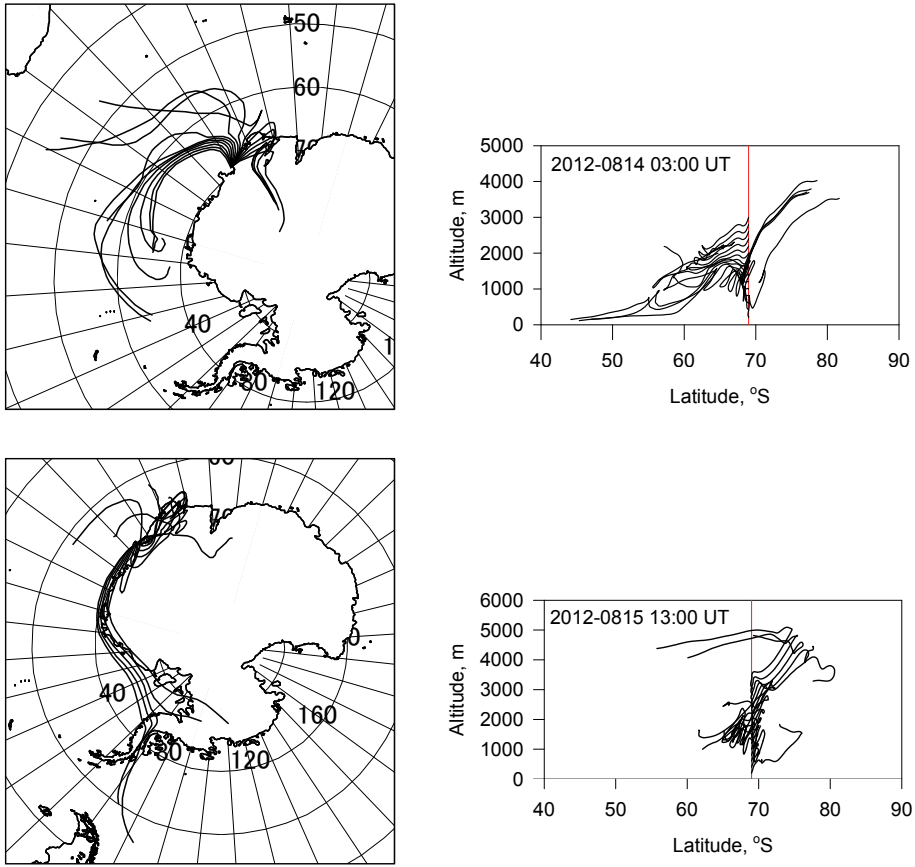

Fig. 4. Examples of 5 day backward trajectory at 03:00 UT on 14 August and at 13:00 UT on 15 August. Red lines represent the latitude of Syowa Station (69° S).

ACPD
13, 26269–26303, 2013

Simultaneous aerosol measurements of unusual aerosol enhancement

K. Hara et al.

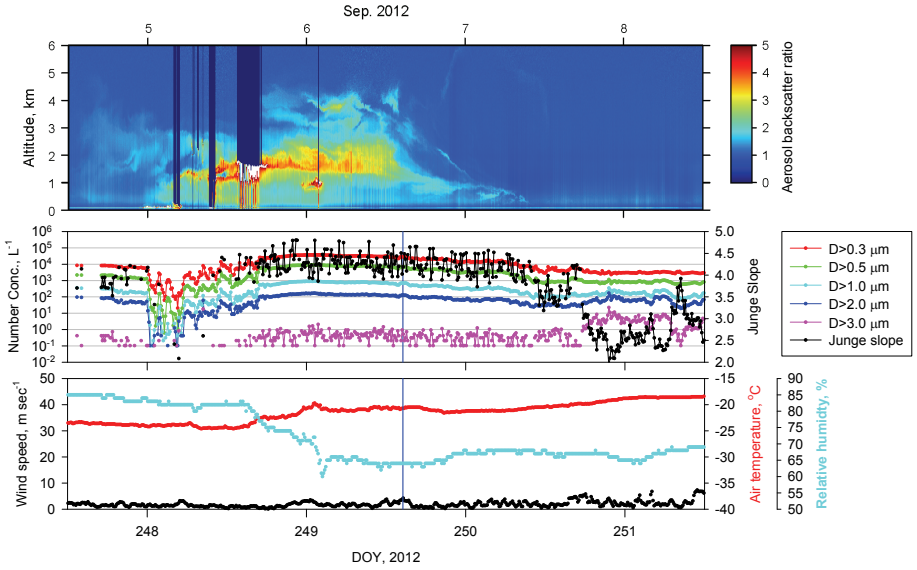

Fig. 5. Short-term variations of the aerosol backscatter ratio, aerosol number concentrations near the surface, wind speed, air temperature, and relative humidity on 4–7 September 2012 at Syowa Station, Antarctica.

ACPD
13, 26269–26303, 2013

Simultaneous aerosol measurements of unusual aerosol enhancement

K. Hara et al.

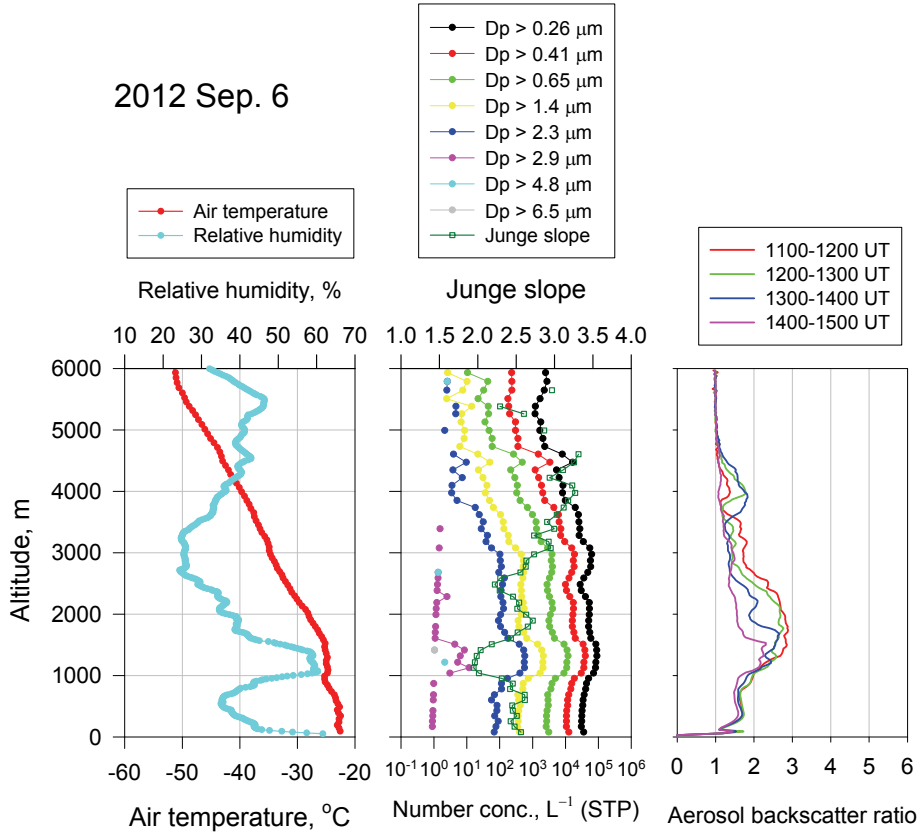

Fig. 6. Vertical variations of air temperature, relative humidity, aerosol number concentrations, Junge slope, and backscatter ratio over Syowa Station on 6 September 2012.

ACPD
13, 26269–26303, 2013

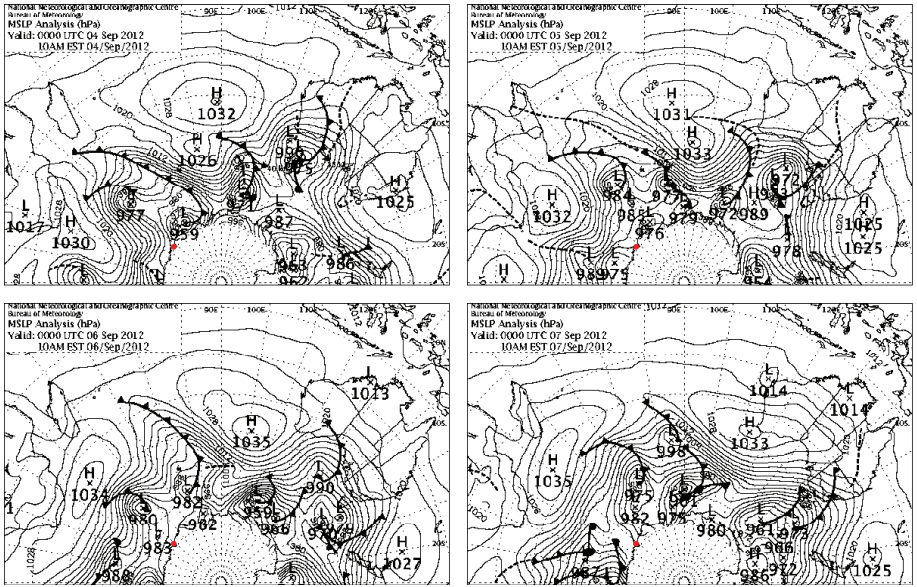

Fig. 7. Surface weather charts of the Indian Ocean sector on 4–7 September 2012 (Bureau of Meteorology, Australia: http://www.bom.gov.au/index.shtml). Red circles represent location of Syowa Station.

ACPD
13, 26269–26303, 2013

Simultaneous aerosol measurements of unusual aerosol enhancement

K. Hara et al.

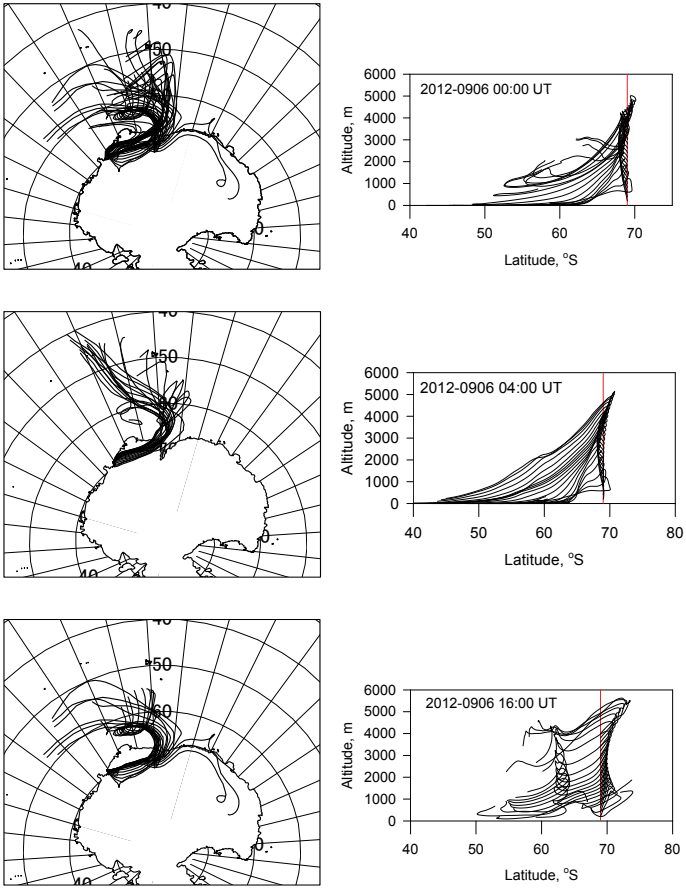

Fig. 8. Examples of 5 day backward trajectory at 00:00 UT on 6 September, at 04:00 UT on 6 September, and at 16:00 UT on 6 September. Red lines represent latitude of Syowa Station (69° S).

ACPD
13, 26269–26303, 2013

Simultaneous aerosol measurements of unusual aerosol enhancement

K. Hara et al.